

Electronic Supplemental Information for:

Low Power Threshold Photochemical Upconversion Using a Zirconium (IV) LMCT Photosensitizer

Mo Yang,^a Sara Sheykhi,^a Yu Zhang,^b Carsten Milsmann,^b and Felix N. Castellano^{*a}

^a Department of Chemistry, North Carolina State University, Raleigh, North Carolina 27695-8204, United States. E-mail: fncastel@ncsu.edu

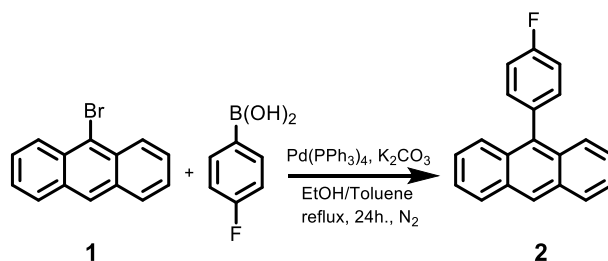
^b C. Eugene Bennett Department of Chemistry, West Virginia University, Morgantown, West Virginia 26506, United States.

Syntheses and Characterization: $\text{Zr}(\text{MesPDP}^{\text{Ph}})_2$ was synthesized and purified as previously reported.¹ All chemicals and solvents were analytical grade, and they were used without purification. Proton nuclear magnetic resonance (¹H NMR) spectra and carbon nuclear magnetic resonance (¹³C NMR) spectra were recorded on a Bruker® Avance NEO-400 spectrometer at 300 K. Proton chemical shifts are expressed as parts per million (ppm, δ scale) and are referenced to residual solvent (CDCl_3 : δ 7.26). Carbon chemical shifts are expressed as parts per million (ppm, δ scale) and are referenced to the solvent (CDCl_3 : δ 77.16). NMR data is presented as follows: chemical shift (δ ppm), multiplicity (s = singlet, d = doublet, dd = doublet of doublets, ddd, doublet of doublet of doublet, t = triplet, m = multiplet), coupling constant (J) in Hertz (Hz), and integration.

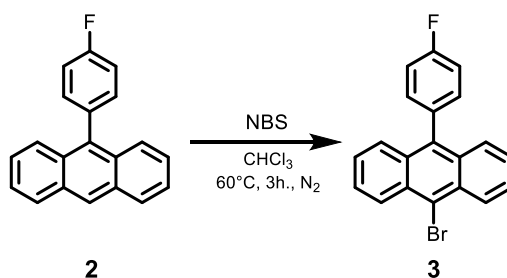
Solution-state DOSY-NMR spectra were obtained on a Bruker Avance 700 MHz instrument operating at a proton frequency of 699.93 MHz, equipped with a 5 mm Bruker TCI probe (H-C-N-D) with Z gradients. All spectra were analyzed with Bruker Topspin 3.2 (Bruker Biospin). $\text{Zr}(\text{MesPDP}^{\text{Ph}})_2$ and CzPA mixture (1 mM) was prepared in deaerated THF-*d*⁸ in 5 mm J-Young NMR tubes. 2D-DOSY diffusion-ordered spectra were obtained using a stimulated echo pulse sequence with bipolar gradients and longitudinal eddy current delay (ledbpgp2s). Scans (16 for each gradient strength) were collected using 1 ms sine-shaped pulses (2 ms bipolar pulse pair) ranging from 0.107 to 5243 G cm⁻¹ in 32 linear increments for $\text{Zr}(\text{MesPDP}^{\text{Ph}})_2$ /CzPA and 20 linear increments for CzPA alone, with a diffusion time of 60 ms, and 16 K time domain data points. Apodization was applied with an exponential function for line broadening of 1.0 Hz, spike suppression factor of 1.0, maximum number of iterations set to 100, noise sensitivity factor of 4, and number of components set to 2. ROESY spectra were acquired on Bruker Avance III 700 MHz instrument operating at a proton frequency of 699.93 MHz, equipped with a 5 mm Bruker TCI probe (H-C-N-D) with Z gradients. These spectra were acquired with the roesyphpp.2 pulse sequence, 8 scans, 256 increments, and 2048-time domain points with a 200 ms spin-lock. All spectra were processed and analyzed with Bruker Topspin 3.2 (Bruker Biospin). Apodization in both dimensions was performed with a shifted sine function and forward linear prediction in the indirect dimension was applied.

a) Synthesis of CzPA: CzPA was prepared according to the method previously reported, with ¹H and ¹³C NMR spectra quantitatively matching those reported in the literature.²

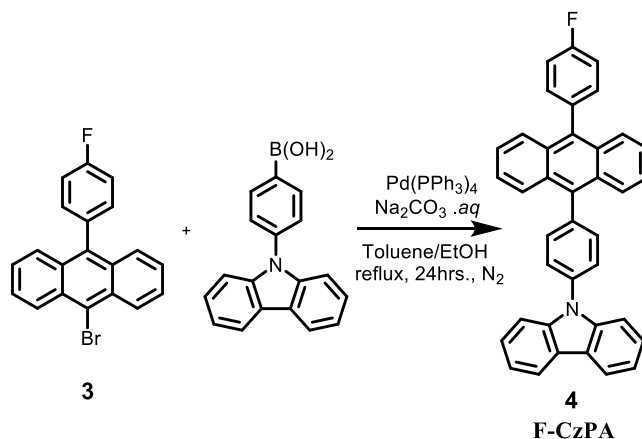
b) Total Synthesis of F-CzPA



F-CzPA was prepared in three steps from **1** following modified literature procedures.³ **2** is synthesized by the Suzuki coupling reaction. 9-bromoanthracene **1** (3 g, 12 mmol, 1 eq.), 4-fluorophenylboronic acid (2.5 g, 18 mmol, 1.5 eq.), Pd(PPh₃)₄ (0.7 g, 0.6 mmol, 0.05 eq.), aqueous K₂CO₃ (2.0 M, 24 mL), ethanol (24 mL), were mixed in a flask containing nitrogen-saturated toluene (100 mL). The reaction mixture was refluxed for 24 hours under a nitrogen atmosphere. After cooling down to room temperature, the reaction mixture was quenched with brine and extracted with toluene. The combined organic layers were dried with anhydrous MgSO₄, filtered, and concentrated in vacuo. The crude product was purified by column chromatography on silica gel with hexane as the eluent to give the desired compound **2** (2.9 g, 10.8 mmol, 92% yield) as a white solid: ¹H NMR (400 MHz, CDCl₃) δ 8.51 (s, 1H), 8.05 (d, *J* = 8.5 Hz, 2H), 7.64 (d, *J* = 8.8 Hz, 2H), 7.50 – 7.44 (m, 2H), 7.43 – 7.34 (m, 4H), 7.32 – 7.25 (m, 2H); ¹³C NMR (101 MHz, CDCl₃) δ 163.76, 161.31, 135.93, 134.69, 133.00, 132.92, 131.49, 130.51, 128.55, 126.97, 126.69, 125.67, 125.29, 115.67, 115.46; HRMS (EI) *m/z* 272.10 [(M)⁺; calcd for C₂₀H₁₃F: 272.10].

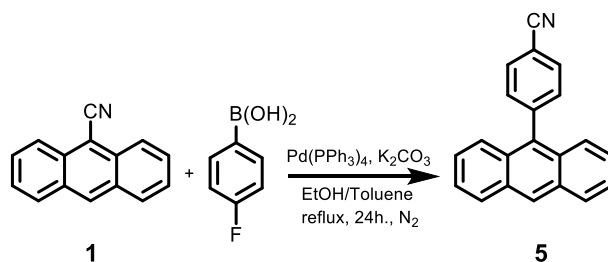


2 (2.9 g, 11 mmol, 1 eq.) was dissolved in 240 mL of chloroform under a nitrogen atmosphere. N-bromosuccinimide (NBS) (2.8 g, 16 mmol, 1.5 eq.) was added to the reaction mixture. The mixture was heated to 60°C for 3 hours under nitrogen. After it was cooled to room temperature, the reaction mixture was evaporated. The residue was redissolved in acetone, and the solution then was added to cold methanol. The resulting precipitate was filtered and washed with methanol to give the desired compound **3** (2.9 g, 8.3 mmol, 78% yield) as a yellow solid: ¹H NMR (400 MHz, CDCl₃) δ 8.59 (d, *J* = 8.9 Hz, 2H), 7.57 (ddd, *J* = 11.0, 7.7, 5.0 Hz, 4H), 7.40 – 7.31 (m, 4H), 7.29 – 7.22 (m, 2H); ¹³C NMR (101 MHz, CDCl₃) δ 163.86, 161.41, 136.64, 134.32, 134.28, 132.91, 132.83, 131.29, 130.36, 128.08, 127.21, 127.11, 126.72, 125.88, 123.21, 115.78, 115.57; HRMS (EI) *m/z* 350.01 [(M)⁺; calcd for C₂₀H₁₂BrF: 350.2].



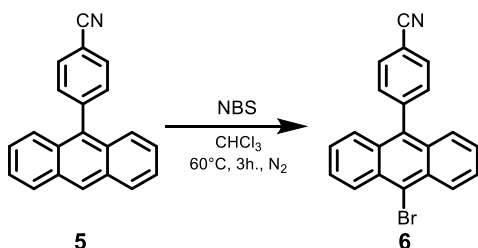
9-(4-(10-(4-fluorophenyl)anthracen-9-yl)phenyl)-9H-carbazole (**F-CzPA**) **4** was synthesized by the Suzuki coupling reaction. **3** (2.8 g, 8 mmol, 1 eq.), 4-(9H-carbazol-9-yl)phenylboronic acid (3.4 g, 12 mmol, 1.5 eq.), Pd(PPh₃)₄ (0.3 g, 0.3 mmol, 0.05 eq.), aqueous K₂CO₃ (2.0 M, 22 mL), ethanol (22 mL), were mixed in a flask containing nitrogen-saturated toluene (100 mL). The reaction mixture was refluxed for 24 hours under a nitrogen atmosphere. After cooling down to room temperature, the reaction mixture was quenched with brine and extracted with toluene. The combined organic layers were dried with anhydrous MgSO₄, filtered, and concentrated in vacuo. The crude product was purified by column chromatography on silica gel (0% DCM in hexanes → 100% DCM) as the eluent. The product was further purified by recrystallization in toluene followed by sublimation under vacuum to give the desired compound **4** (**F-CzPA**) (3.6 g, 7.0 mmol, 90% yield) as a white solid: ¹H NMR (400 MHz, CDCl₃) δ 8.22 (d, *J* = 7.7 Hz, 2H), 7.84 (dd, *J* = 8.2, 4.8 Hz, 4H), 7.72 (d, *J* = 8.5 Hz, 4H), 7.68 (d, *J* = 8.2 Hz, 2H), 7.53 – 7.30 (m, 12H); ¹³C NMR (101 MHz, CDCl₃) δ 141.04, 138.28, 137.30, 136.48, 133.08, 133.00, 132.96, 130.27, 130.13, 127.11, 127.02, 126.97, 126.20, 125.57, 125.49, 123.72, 120.58, 120.29, 115.80, 115.59, 110.09; HRMS (EI) *m/z* 513.19 [(M)⁺; calcd for C₃₈H₂₄FN: 513.2].

c) Total Synthesis of CN-CzPA

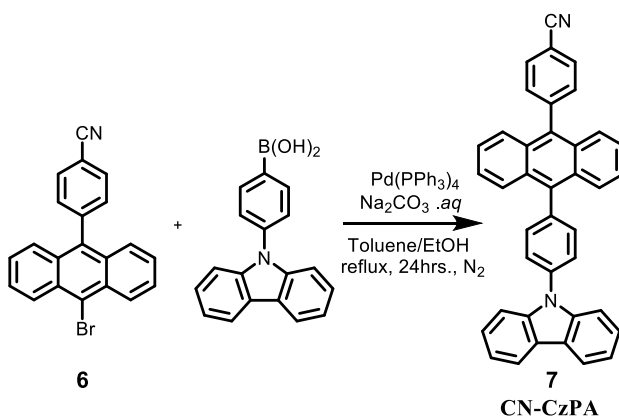


CN-CzPA was prepared in three steps from **1** following modified literature procedures.³ **5** was synthesized by the Suzuki coupling reaction. 9-Bromoanthracene **1** (3 g, 12 mmol, 1 eq.), 4-cyanophenylboronic acid (2.6 g, 18 mmol, 1.5 eq.), Pd(PPh₃)₄ (0.7 g, 0.6 mmol, 0.05 eq.), aqueous K₂CO₃ (2.0 M, 24 mL), ethanol (24 mL), were mixed in a flask containing nitrogen-saturated toluene (100 mL). The reaction mixture was refluxed for 24 hours under a nitrogen atmosphere. After cooling down to room temperature, the reaction mixture was quenched with brine and extracted with toluene. The combined organic layers were dried with anhydrous MgSO₄, filtered, and concentrated in vacuo. The crude product was purified by column chromatography on silica

gel with hexane as the eluent to give the desired compound **5** (2.7 g, 9.7 mmol, 84% yield) as a pale yellow solid: $^1\text{H NMR}$ (400 MHz, CDCl_3) δ 8.54 (s, 1H), 8.06 (d, $J = 8.5$ Hz, 2H), 7.91 – 7.86 (m, 2H), 7.59 – 7.54 (m, 2H), 7.53 – 7.45 (m, 4H), 7.38 (ddd, $J = 8.6, 6.6, 1.2$ Hz, 2H); $^{13}\text{C NMR}$ (101 MHz, CDCl_3) δ 144.36, 134.59, 132.40, 132.35, 131.37, 129.85, 128.73, 127.78, 126.21, 126.01, 125.46, 119.05, 111.75; **HRMS** (EI) m/z 279.10 $[(\text{M})^+]$; calcd for $\text{C}_{21}\text{H}_{13}\text{N}$: 279.10].



5 (2.6 g, 9.3 mmol, 1 eq.) was dissolved in 240 mL of chloroform under nitrogen. N-bromosuccinimide (NBS) (2.5 g, 14 mmol, 1.5 eq.) was added to the reaction mixture. The mixture was heated to 60°C for 3 hours under nitrogen. After it was cooled to room temperature, the reaction mixture was evaporated. The residue was redissolved in acetone, and the resulting solution was added to cold methanol. The resulting precipitate was filtered and washed with methanol to give the desired compound **6** (2.9 g, 8.1 mmol, 88% yield) a yellow solid: $^1\text{H NMR}$ (400 MHz, CDCl_3) δ 8.64 (d, $J = 8.9$ Hz, 2H), 7.92 – 7.87 (m, 2H), 7.62 (ddd, $J = 8.9, 6.4, 1.2$ Hz, 2H), 7.57 – 7.53 (m, 2H), 7.49 (d, $J = 8.6$ Hz, 2H), 7.41 (ddd, $J = 8.8, 6.4, 1.1$ Hz, 2H); $^{13}\text{C NMR}$ (101 MHz, CDCl_3) δ 143.90, 135.25, 132.46, 132.23, 130.57, 130.30, 128.30, 127.27, 126.56, 126.41, 124.09, 118.87, 112.09; **HRMS** (EI) m/z 357.02 $[(\text{M})^+]$; calcd for $\text{C}_{21}\text{H}_{12}\text{BrN}$: 357.10].



4-(10-(4-(9H-carbazol-9-yl)phenyl)anthracen-9-yl)benzonitrile (**CN-CzPA**) **7** was synthesized by the Suzuki coupling reaction. **6** (2.0 g, 5.4 mmol, 1 eq.), N-phenylcarbazole boronic acid (2.8 g, 8 mmol, 1.5 eq.), $\text{Pd}(\text{PPh}_3)_4$ (0.3 g, 0.3 mmol, 0.05 eq.), aqueous K_2CO_3 (2.0 M, 22 mL), ethanol (22 mL), were mixed in a flask containing nitrogen-saturated toluene (100 mL). The reaction mixture was refluxed for 24 hours under a nitrogen atmosphere. After cooling down to room temperature, the reaction mixture was quenched with brine and extracted with toluene. The combined organic layers were dried with anhydrous MgSO_4 , filtered, and concentrated in vacuo. The crude product was purified by column chromatography on silica gel with hexane (0% DCM in hexanes \rightarrow 100% DCM) as the eluent. The product was further purified by recrystallization in

toluene followed by sublimation under vacuum to give the desired compound **7 (CN-CzPA)** (2.4 g, 4.6 mmol, 80% yield) as a pale yellow solid: **¹H NMR** (400 MHz, CDCl₃) δ 8.21 (d, *J* = 7.7 Hz, 2H), 7.94 (d, *J* = 8.2 Hz, 2H), 7.85 (dd, *J* = 10.6, 8.3 Hz, 4H), 7.73 – 7.64 (m, 6H), 7.61 – 7.57 (m, 2H), 7.54 – 7.40 (m, 6H), 7.36 (dd, *J* = 11.0, 3.9 Hz, 2H); **¹³C NMR** (101 MHz, CDCl₃) δ 144.56, 140.99, 137.92, 137.45, 137.33, 135.12, 132.86, 132.51, 132.43, 130.05, 129.62, 127.16, 127.13, 126.35, 126.21, 126.01, 125.73, 123.74, 120.60, 120.33, 119.03, 111.89, 110.04; **HRMS** (EI) *m/z* 520.19 [(M)⁺; calcd for C₃₉H₂₄N₂: 520.2].

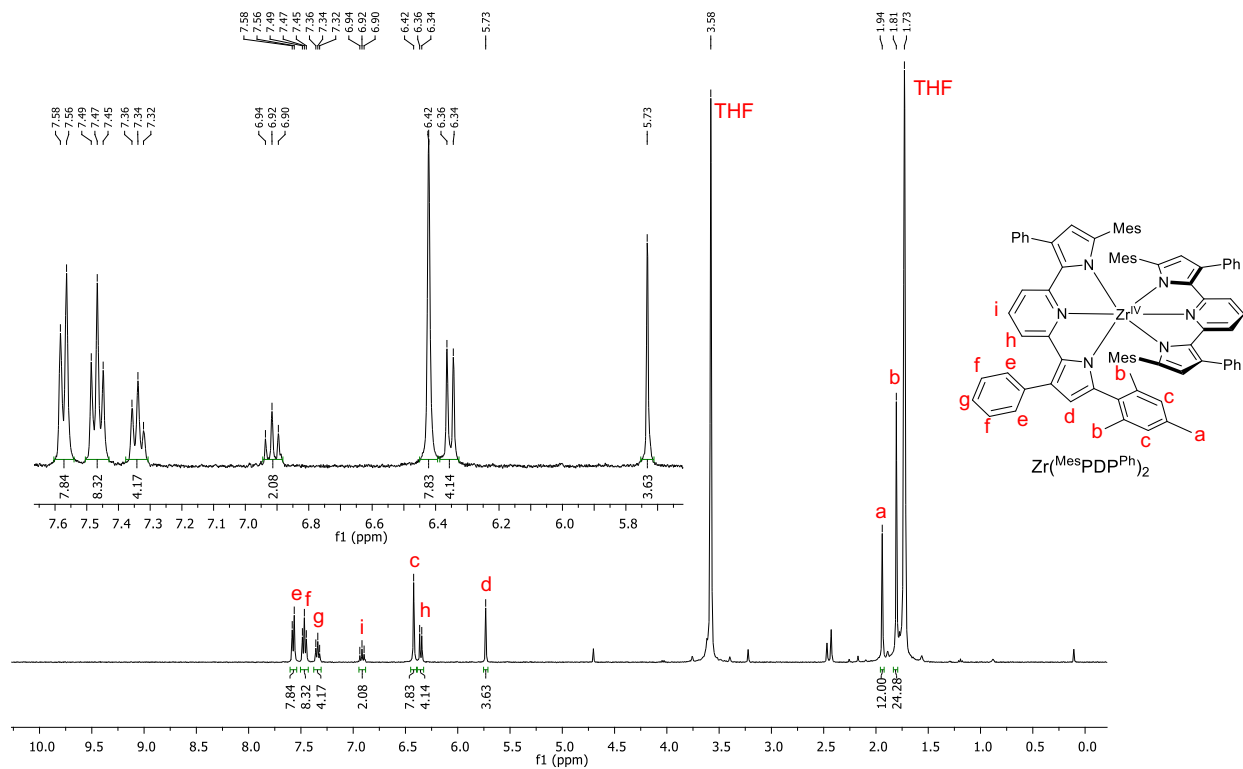


Fig. S1 700 MHz ^1H NMR spectrum of $\text{Zr}(\text{MesPDPPh})_2$ in THF at 300 K.

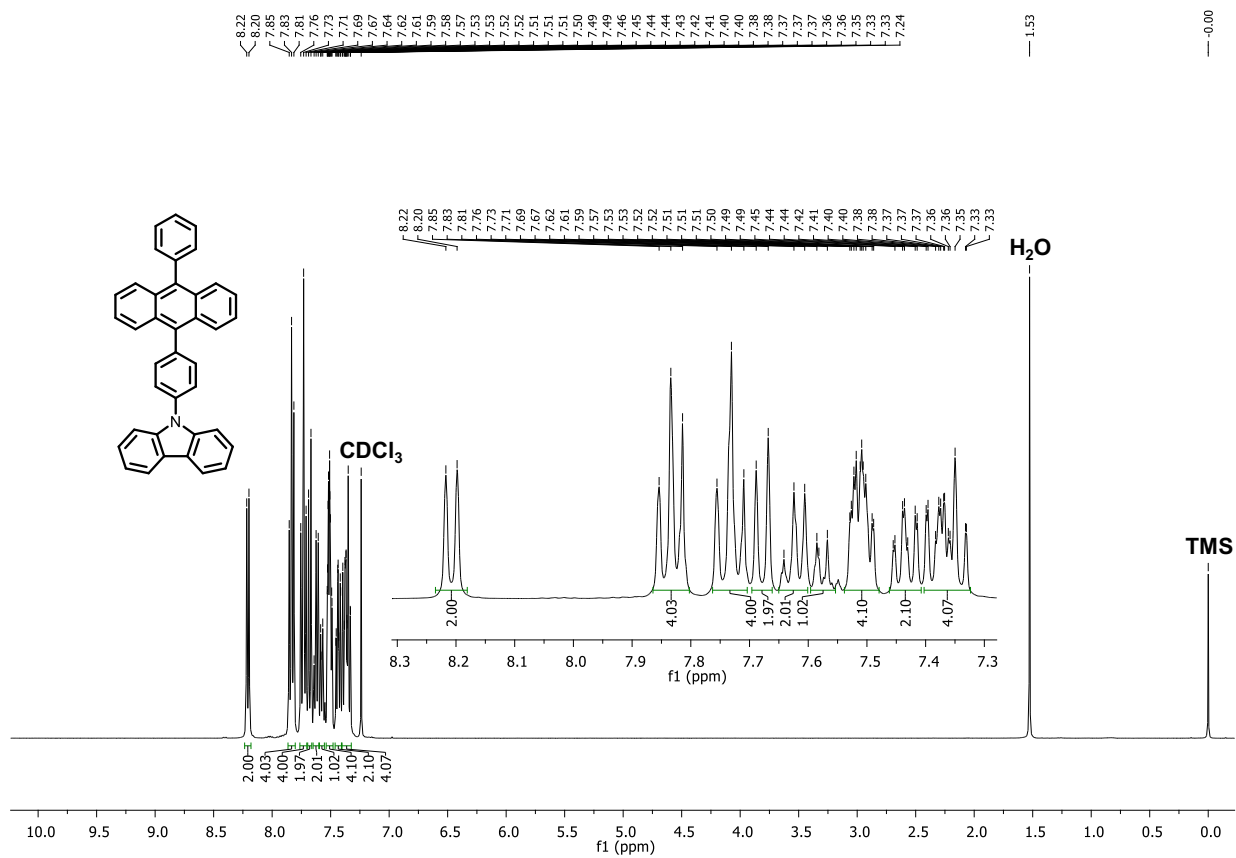


Fig. S2 400 MHz ^1H NMR spectrum of CzPA in CDCl_3 at 300 K.

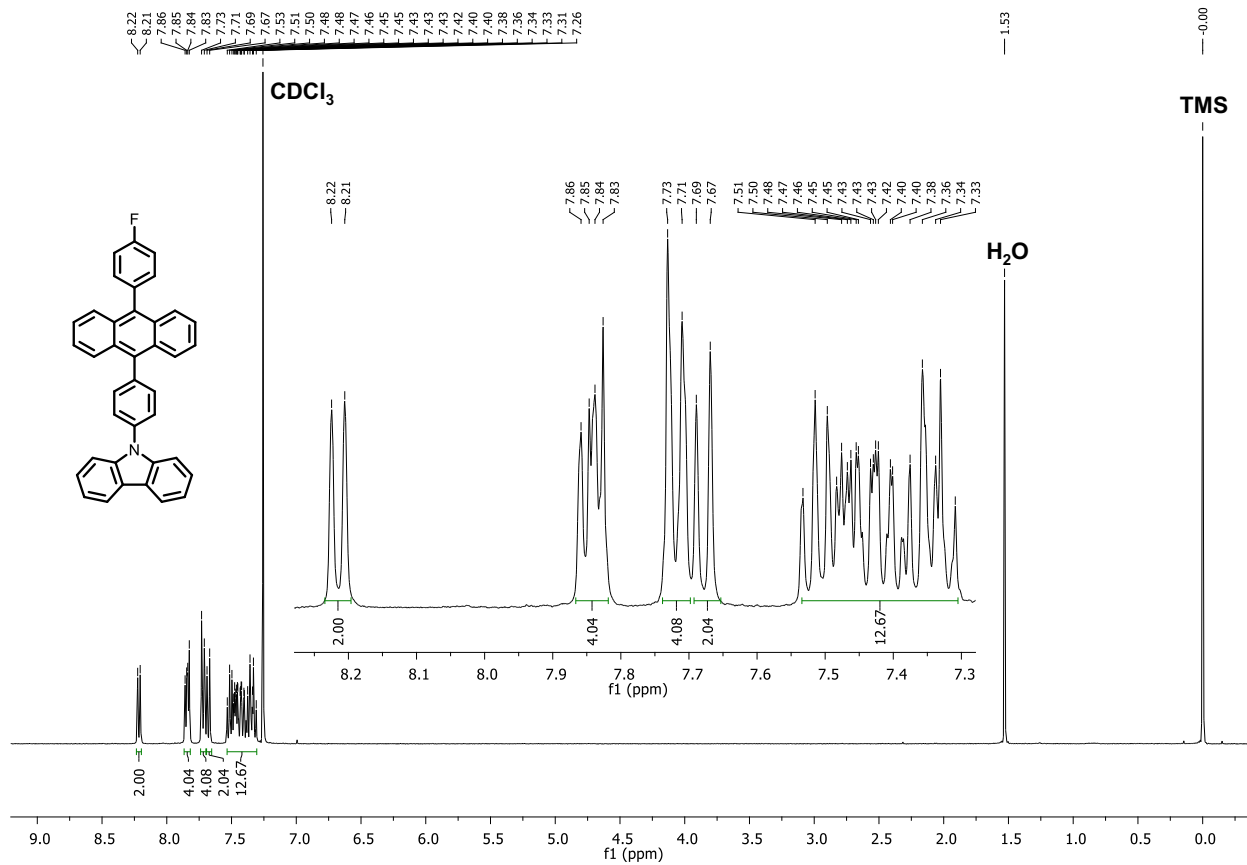


Fig. S4 400 MHz ^1H NMR spectrum of F-CzPA in CDCl_3 at 300 K.

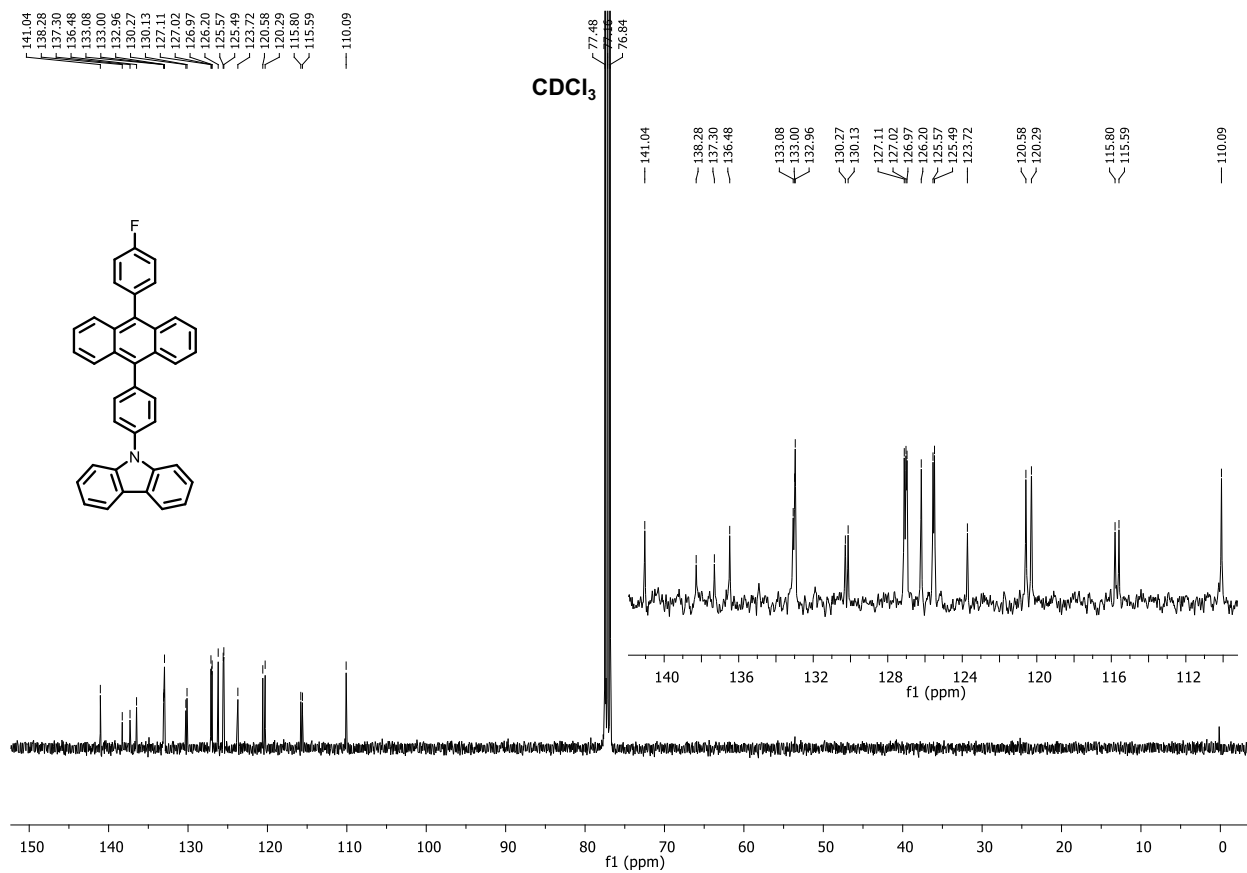


Fig. S5 125 MHz ¹³C NMR spectrum of F-CzPA in CDCl₃ at 300 K.

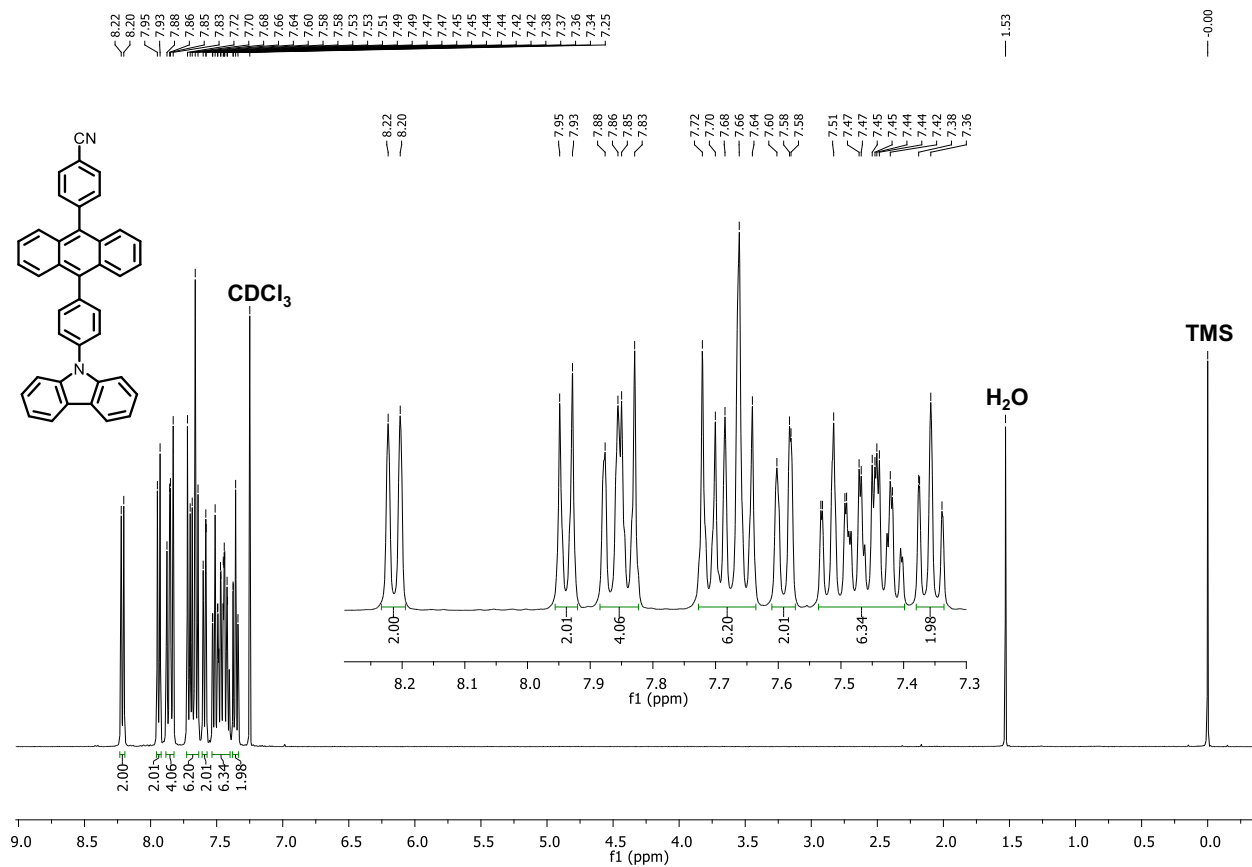


Fig. S6 400 MHz ^1H NMR spectrum of CN-CzPA in CDCl_3 at 300 K.

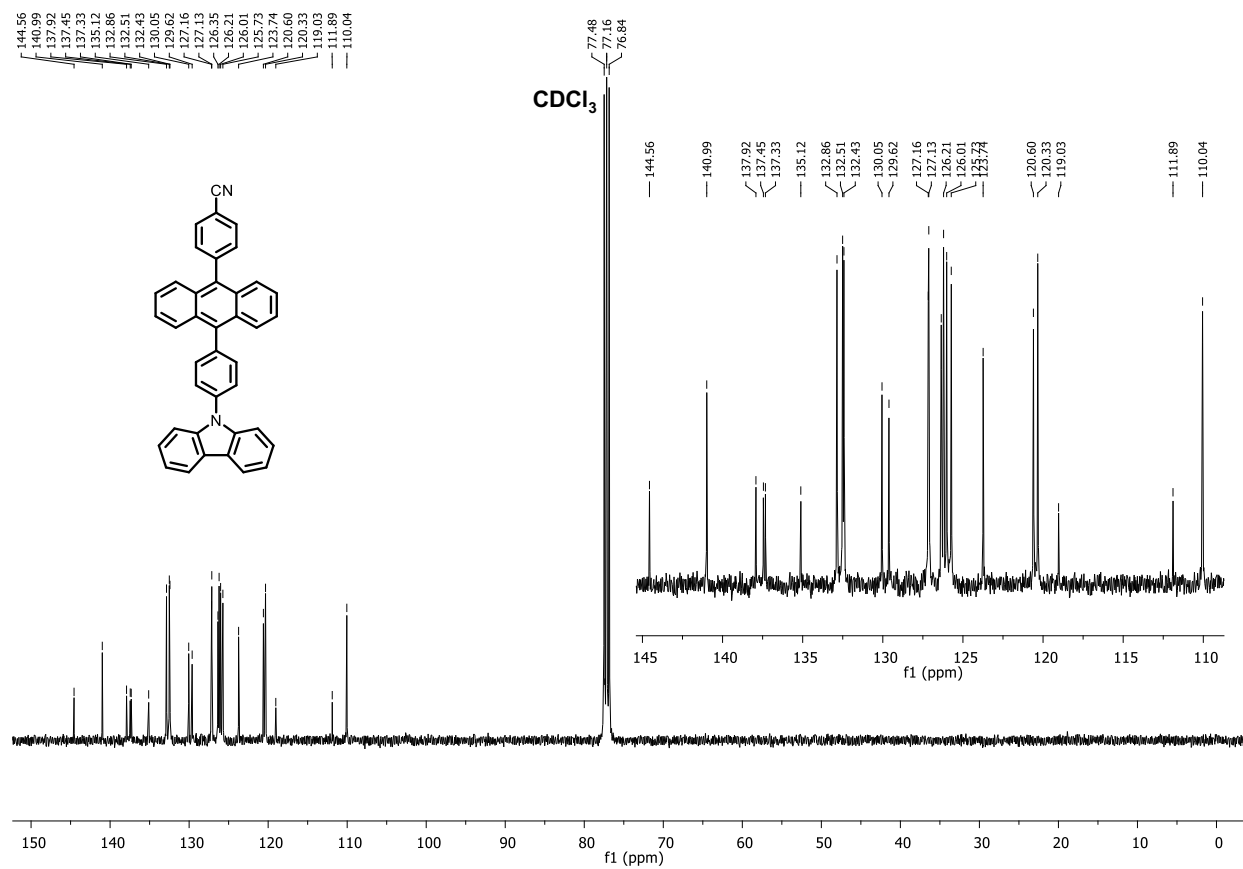


Fig. S7 125 MHz ¹³C NMR spectrum of CN-CzPA in CDCl₃ at 300 K.

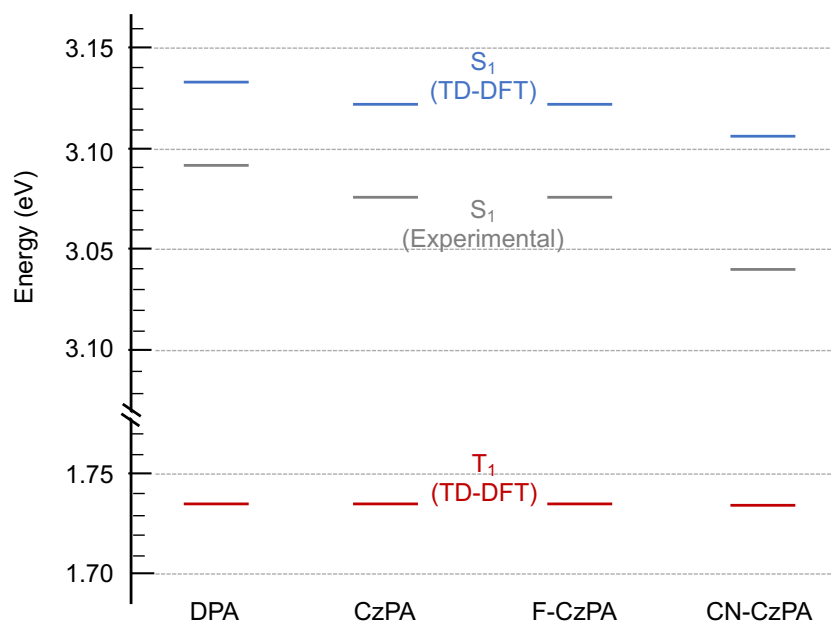


Fig. S8 Experimental (grey) singlet state energies estimated from the crossing point of the normalized absorbance and fluorescence spectra. The trend in the TD-DFT calculated singlet state energies (blue) is in well³¹ agreement with experimental observations. The red bars show the TD-DFT calculated energies of the T₁ states.

Table S1 Optical properties and calculated energies of the acceptors/annihilators using DFT calculations with the TD-B3LYP/6-31G(d) functional.

Annihilator	$\lambda_{\text{abs}}^{\text{a}}$ (nm)	$\lambda_{\text{em}}^{\text{a}}$ (nm)	S ₁ ^b (eV)	S ₁ ^c (eV)	T ₁ ^c (eV)	T ₂ ^c (eV)	HOMO ^c (eV)	LUMO ^c (eV)	E _g ^c (eV)
DPA	374	408	3.092	3.133	1.737	3.269	-5.269	-1.772	3.497
CzPA	375	418	3.077	3.122	1.736	3.191	-5.309	-1.818	3.491
F-CzPA	374	419	3.077	3.122	1.736	3.191	-5.337	-1.847	3.490
CN-CzPA	374	435	3.039	3.106	1.734	3.190	-5.410	-1.930	3.480

^aHighest energy maximum in the absorbance/photoluminescence spectra. ^bEstimated from crossing points of absorbance and photoluminescence spectra. ^cCalculated by the TD-B3LYP/6-31G(d) method using Gaussian '16.

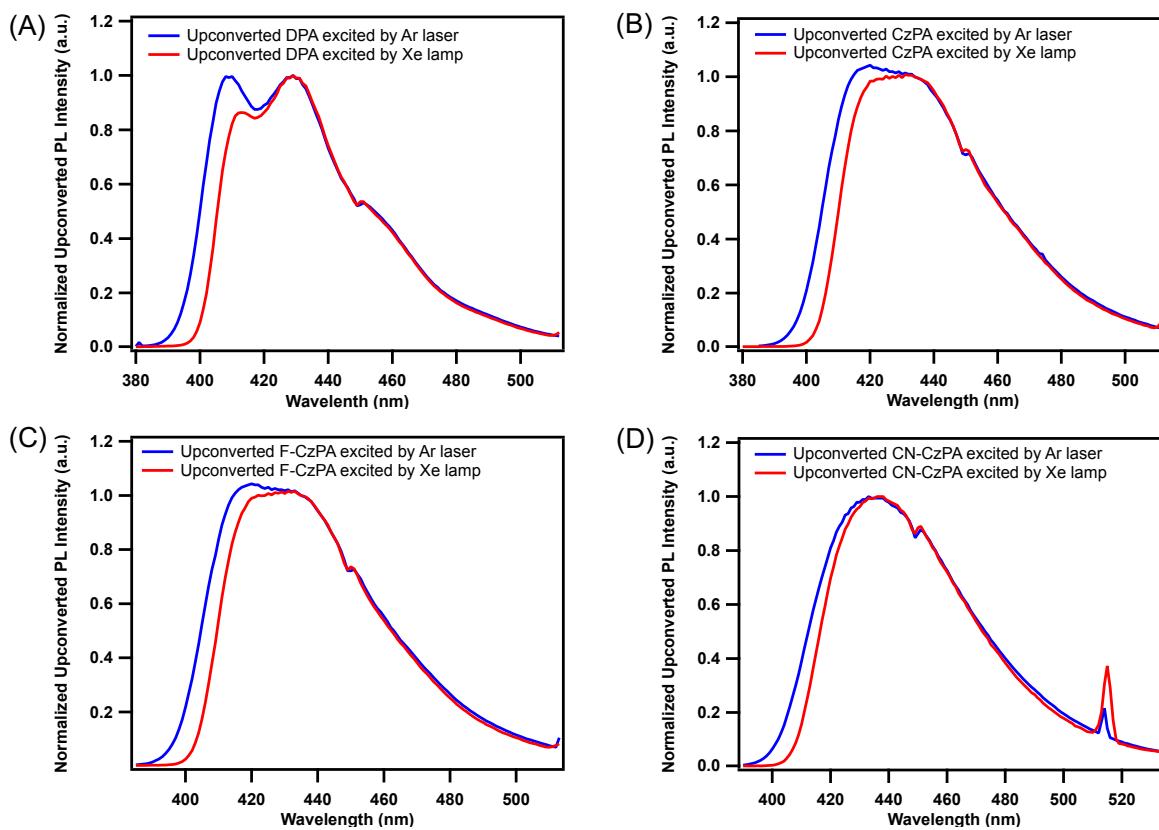


Fig. S9 Normalized upconverted fluorescence spectra of the acceptors/annihilators sensitized by $\text{Zr}(\text{MesPDP}^{\text{Ph}})_2$ under Ar^+/Kr^+ ion continuous-wave laser (blue) and Xe lamp/monochromator (red) excitation, $\lambda_{\text{exc}} = 514.5 \text{ nm}$.

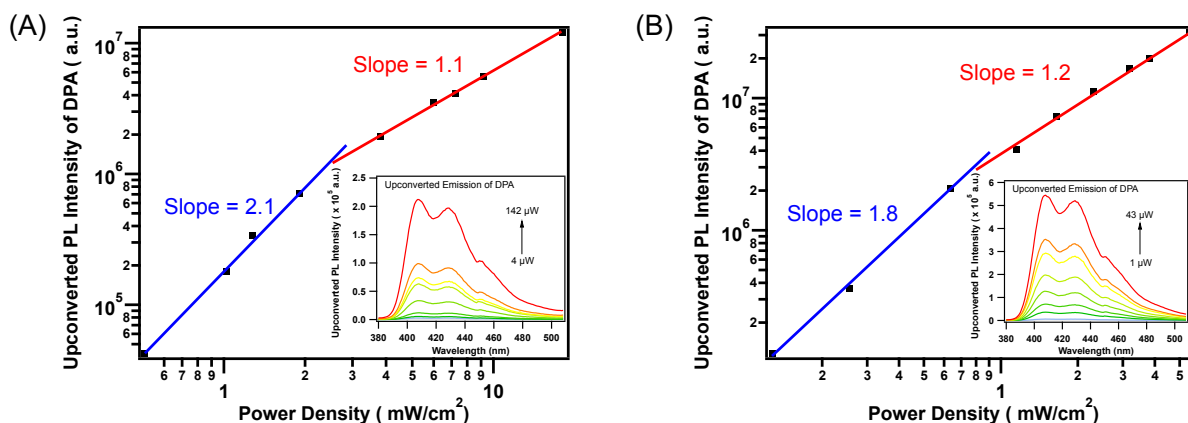


Fig. S10 Double logarithmic plot of upconverted photoluminescence intensities of DPA as a function of 514.5 nm incident laser power densities. Solution samples were under unoptimized quenching conditions: (A) 2.05 μM DPA sensitized by $\text{Zr}(\text{MesPDP}^{\text{Ph}})_2$ ($\text{OD}_{514 \text{ nm}} \sim 0.05$, 14% quenching efficiency) in deaerated THF, and (B) 12.5 μM DPA sensitized by $\text{Zr}(\text{MesPDP}^{\text{Ph}})_2$ ($\text{OD}_{514 \text{ nm}} \sim 0.08$, 50% quenching efficiency) in deaerated THF. The solid lines are the linear fits with slopes of ~ 1 (red) and ~ 2 (blue), implying the linear response in the high-power regime and the quadratic response in the low power regime, respectively. The insets show upconverted photoluminescence spectra of the corresponding solutions at different incident laser powers.

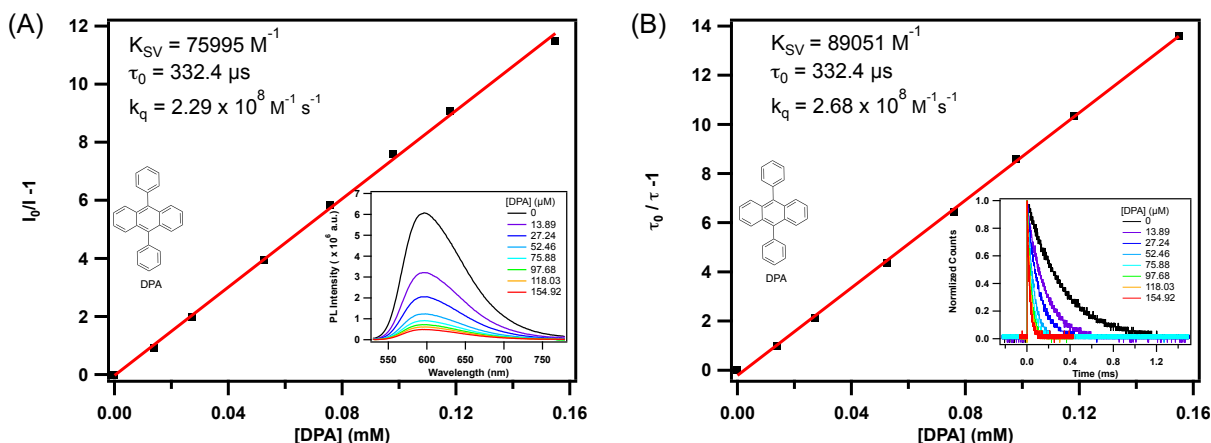


Fig. S11 Stern-Volmer analyses of photoluminescence intensities (A) and lifetimes (B) data for $\text{Zr}(\text{MesPDP}^{\text{Ph}})_2$ quenched by DPA in deaerated THF. Insets are photoluminescence intensity decay (A) and time-resolved photoluminescence decay (B) of $\text{Zr}(\text{MesPDP}^{\text{Ph}})_2$ at different DPA acceptor/annihilator concentrations, respectively.

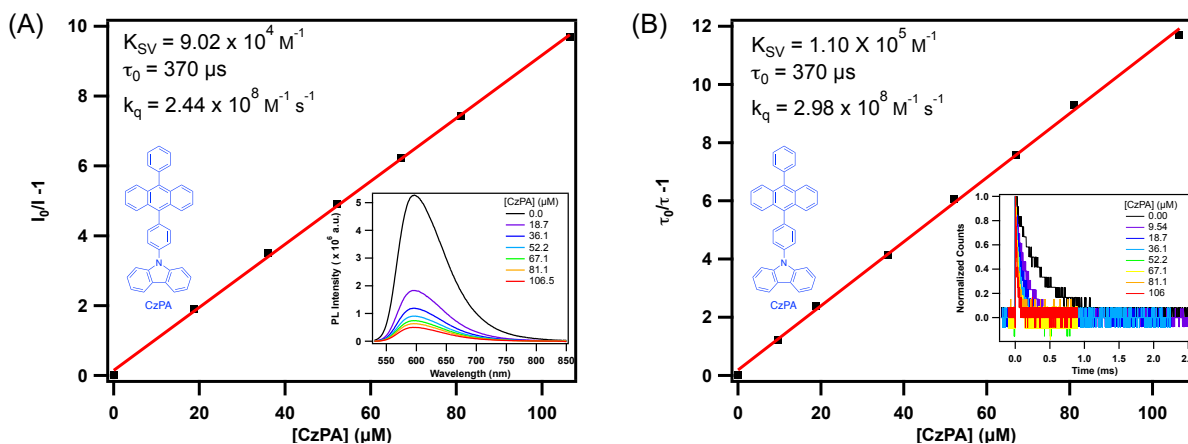


Fig. S12 Stern-Volmer analyses of photoluminescence intensities (A) and lifetimes (B) data for $Zr(\text{MesPDP}^{\text{Ph}})_2$ quenched by CzPA in deaerated THF. Insets are photoluminescence intensity decay (A) and time-resolved photoluminescence decay (B) of $Zr(\text{MesPDP}^{\text{Ph}})_2$ at different CzPA acceptor/annihilator concentrations, respectively.

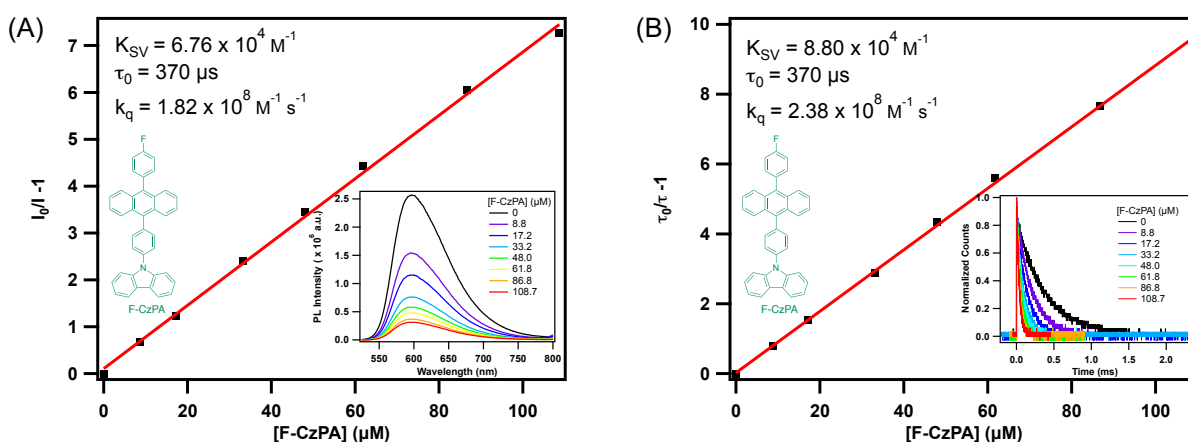


Fig. S13 Stern-Volmer analyses of photoluminescence intensities (A) and lifetimes (B) data for $Zr(\text{MesPDP}^{\text{Ph}})_2$ quenched by F-CzPA in deaerated THF. Insets are photoluminescence intensity decay (A) and time-resolved photoluminescence decay (B) of $Zr(\text{MesPDP}^{\text{Ph}})_2$ at different F-CzPA acceptor/annihilator concentrations, respectively.

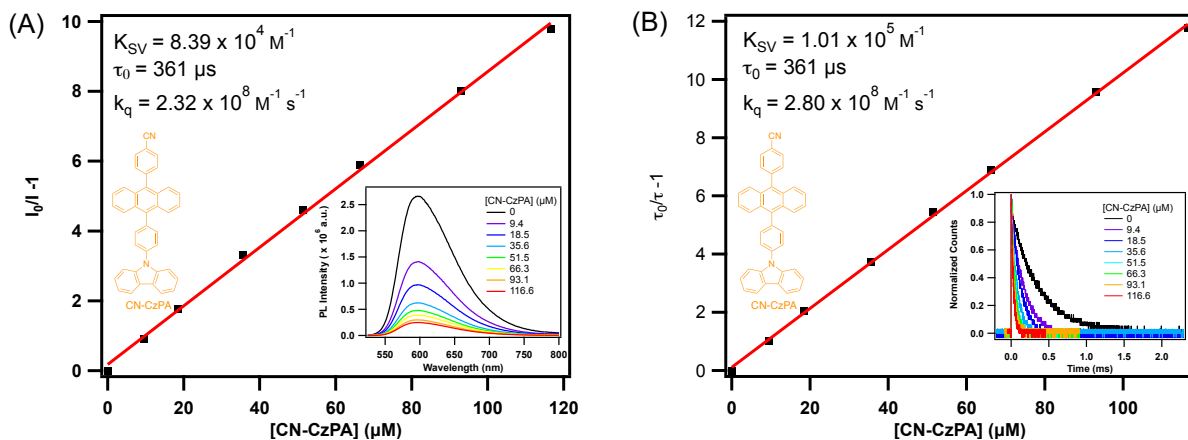


Fig. S14 Stern-Volmer analyses of photoluminescence intensities (A) and lifetimes (B) data for $Zr^{(MesPDPPh)_2}$ quenched by CN-CzPA in deaerated THF. Insets are photoluminescence intensity decay (A) and time-resolved photoluminescence decay (B) of $Zr^{(MesPDPPh)_2}$ at different CN-CzPA acceptor/annihilator concentrations, respectively.

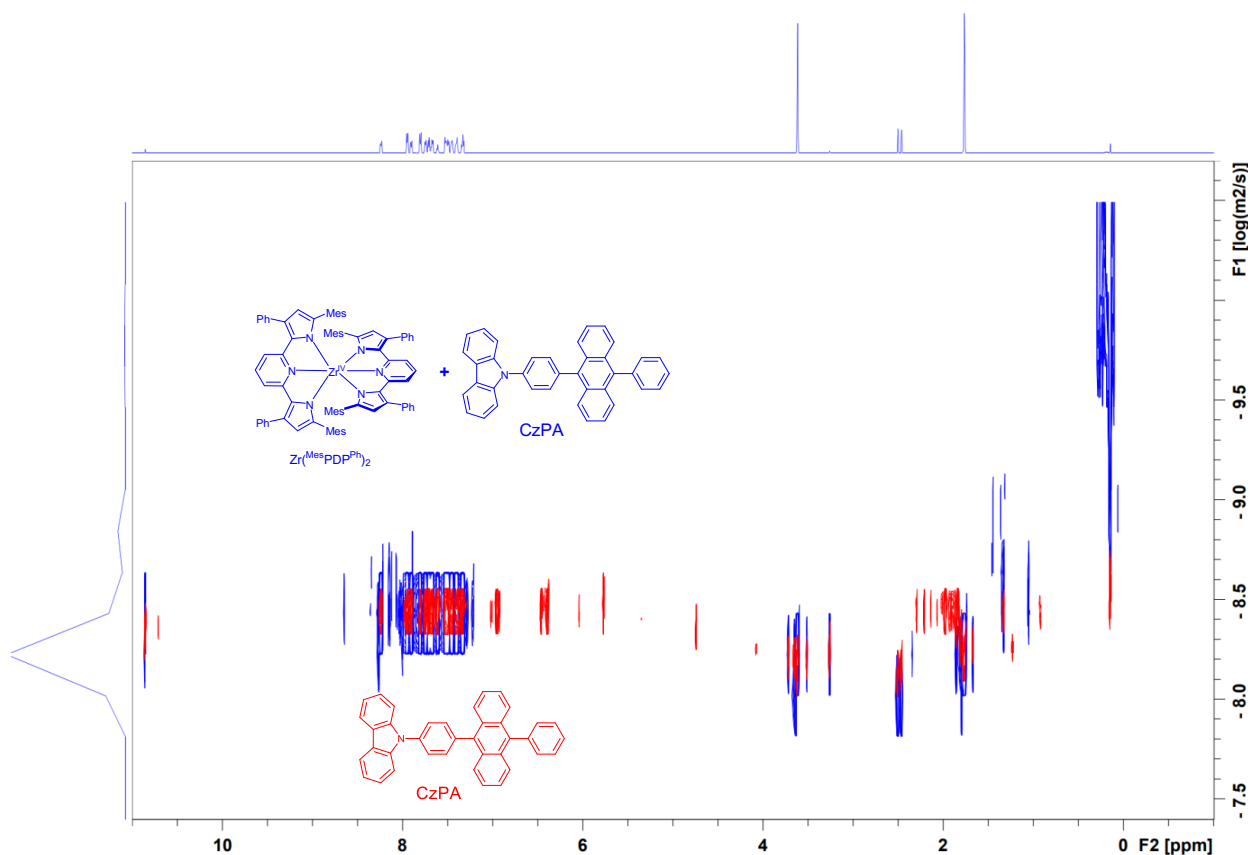


Fig. S15 DOSY spectrum of CzPA (red) and mixture of $Zr^{(MesPDPPh)_2}$ /CzPA (blue) in deaerated THF- d_8 at 25 °C.

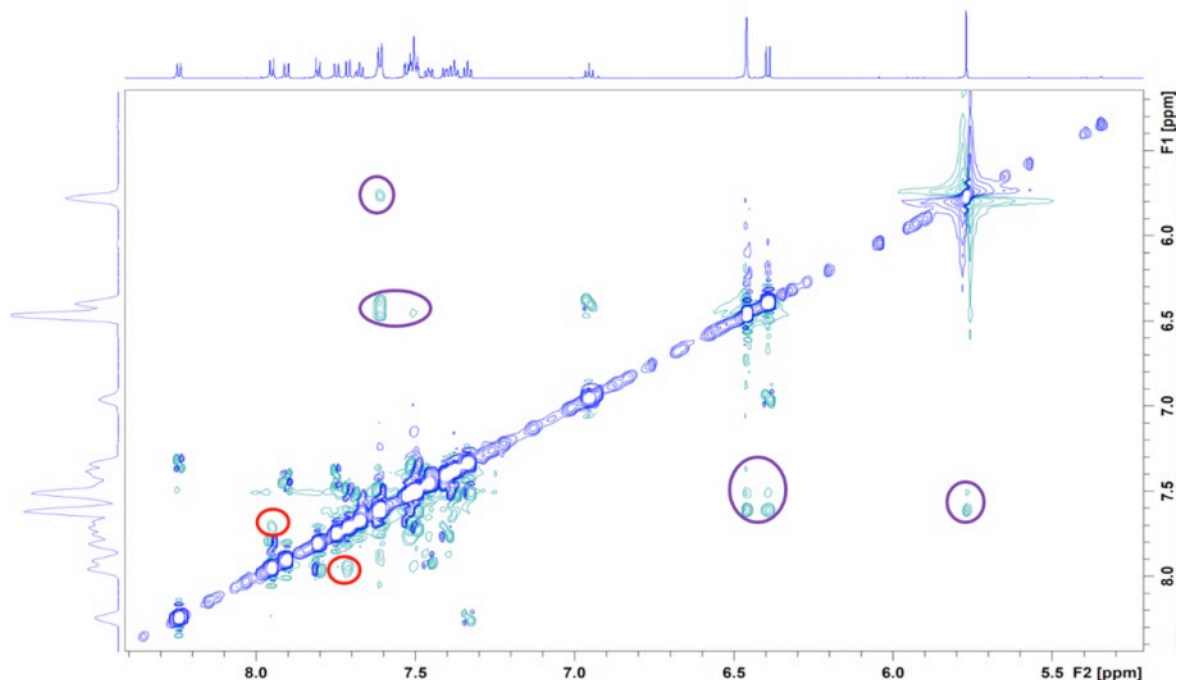


Fig. S16 ROESY spectrum of $\text{Zr}(\text{MesPDP}^{\text{Ph}})_2$ and CzPA mixture in deaerated $\text{THF-}d_8$ at 25°C . Intramolecular ROESY crosspeaks: $\text{Zr}(\text{MesPDP}^{\text{Ph}})_2$ (purple circle) and CzPA (red circle). There are no clearly identifiable intermolecular ROESY cross peaks.

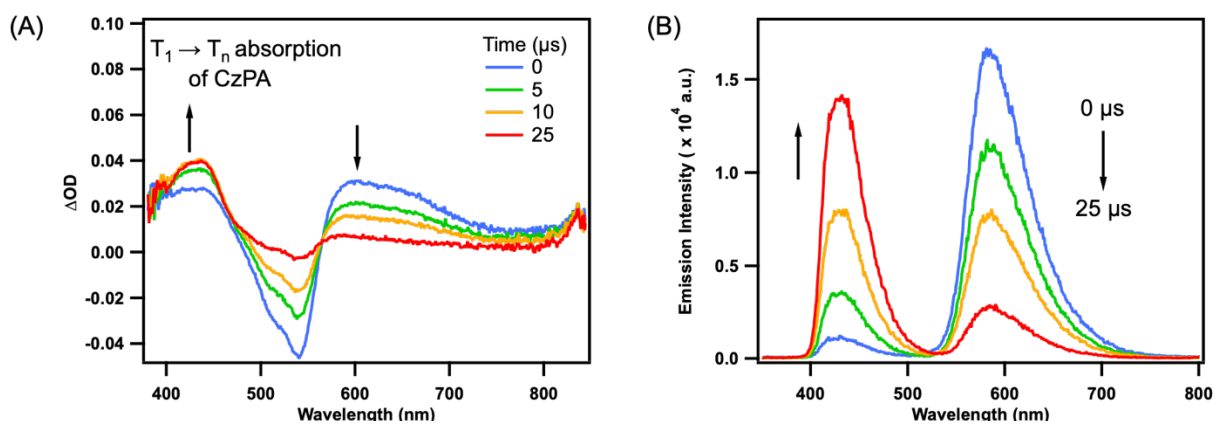


Fig. S17 Transient absorption difference spectrum (A) and time-resolved photoluminescence spectrum (B) of $\text{Zr}(\text{MesPDP}^{\text{Ph}})_2$ ($\text{OD}_{514\text{ nm}} = 0.35$) and 0.25 mM CzPA in deaerated THF at several delay times following 514 nm pulsed laser excitation ($\sim 2\text{ mJ/pulse}$) with several delay times.

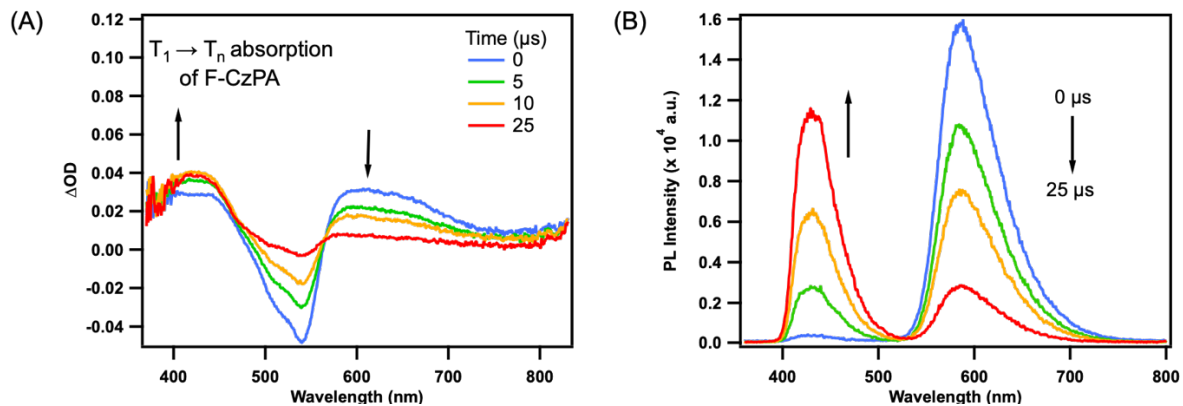


Fig. S18 Transient absorption difference spectrum (A) and time-resolved photoluminescence spectrum (B) of $Zr^{(MesPDP^{Ph})_2}$ ($OD_{514\text{ nm}} = 0.45$) and 0.25 mM F-CzPA in deaerated THF at several delay times following 514 nm pulsed laser excitation (~ 2 mJ/pulse) with several delay times.

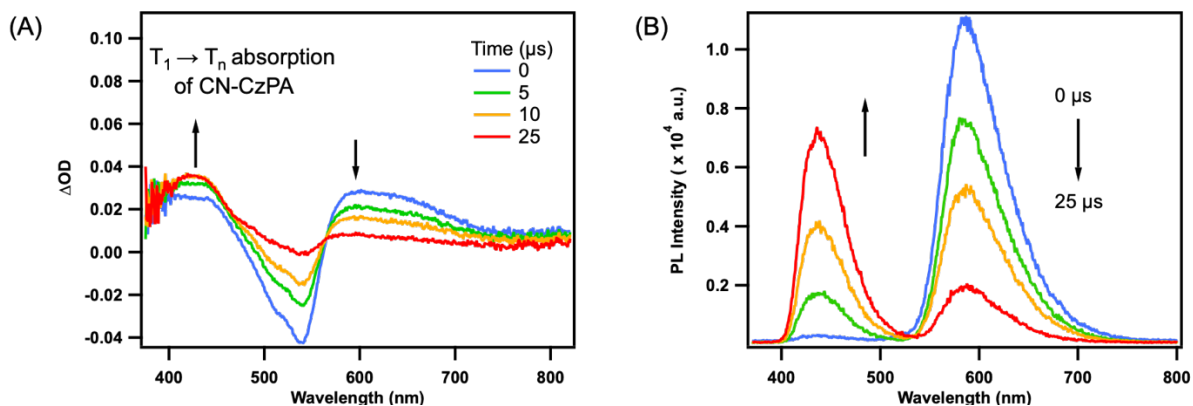


Fig. S19 Transient absorption difference spectrum (A) and time-resolved photoluminescence spectrum (B) of $Zr^{(MesPDP^{Ph})_2}$ ($OD_{514\text{ nm}} = 0.4$) and 0.25 mM CN-CzPA in deaerated THF at several delay times following 514 nm pulsed laser excitation (~ 2 mJ/pulse) with several delay times.

Determination of the Triplet Decay (k_T) and the Triplet-Triplet Annihilation (k_{TTA}) rate Constants: Subsequent to the conversion of the excited sensitizer population to acceptor/annihilator triplets, the sensitized triplets' decay with parallel first- and second-order kinetics:⁴⁻⁶

$$\frac{d[{}^3A^*]_t}{dt} = -k_T[{}^3A^*]_t - k_{TTA}[{}^3A^*]_t^2 \quad (S1)$$

where k_T is the first-order triplet decay rate and k_{TTA} is the triplet-triplet annihilation rate constant, and the excited triplet concentration varies with time as $[{}^3A^*]_t$. The analytical solution to Eq. S1 is well established as^{7,4-6,8,9}

$$\frac{[{}^3A^*]_t}{[{}^3A^*]_0} = \frac{1-\beta}{\exp(k_T t)-\beta} \quad (S2)$$

where $\beta = \alpha/(k_T + \alpha)$ and $\alpha = k_{TTA}[{}^3A^*]_0$. $[{}^3A^*]_0$ is the initial sensitized triplet concentration and β equates to the initial fraction of triplet decay occurring through the bimolecular TTA channel. Eq. S2 can be translated to the Eq. S3 in terms of transient absorption signals ΔA . The triplet concentrations $[{}^3A^*]_t$ are directly proportional to their corresponding ΔA values.

$$\Delta A = \frac{\Delta A_0(1-\beta)}{\exp(k_T t)-\beta} \quad (S3)$$

A series of kinetic absorption decay data collected at 450 nm for DPA or 430 nm for CzPA series as a function of pulse energy fit to Eq. S3, yielding the kinetic parameters of ΔA_0 , k_T and β . ΔA_0 can be converted into $[{}^3A^*]_0$ using the extinction coefficient of the triplet excited state (ϵ_T), while k_T and β enable the calculation of k_{TTA} and α ($\beta = \alpha/(k_T + \alpha)$ and $\alpha = k_{TTA}[{}^3A^*]_0$). ϵ_T of DPA is $15,600 \text{ M}^{-1} \text{ cm}^{-1}$ at 450 nm according to the reported averaged ϵ_T in the literature,¹⁰ and ϵ_T of CzPA series acceptors/annihilators were estimated by the Eq. S4:

$$\frac{\epsilon_T(\text{DPA, 450 nm})}{\epsilon_T(\text{CzPA series, 430 nm})} = \frac{\Delta A_{(\text{DPA})}}{\Delta A_{(\text{CzPA series})}} \quad (S4)$$

$\Delta A_{(\text{DPA})}$ and $\Delta A_{(\text{CzPA series})}$ are the maximum changes in optical densities monitored at respective wavelength in the presence of the Zr(IV) sensitizer. All the samples contained 0.25 mM acceptors/annihilators in the presence of the Zr(IV) sensitizer ($\text{OD}_{514 \text{ nm}} = 0.46$) and were excited at 514 nm with 2 mJ pulse energy. The triplet extinction coefficients were measured to be $\epsilon_{T(\text{CzPA, 430nm})} = 14,600 \text{ M}^{-1} \text{ cm}^{-1}$, $\epsilon_{T(\text{CzPA, 430nm})} = 14,700 \text{ M}^{-1} \text{ cm}^{-1}$, and $\epsilon_{T(\text{CzPA, 430nm})} = 13,500 \text{ M}^{-1} \text{ cm}^{-1}$.

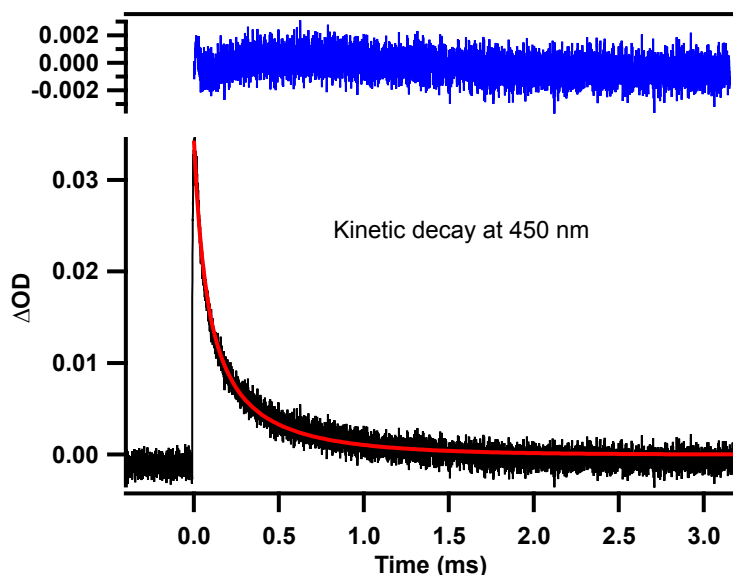


Fig. S20. Representative transient absorption kinetic decay of ${}^3\text{DPA}^*$ at 450 nm produced using 514 nm excitation (2.9 mJ/pulse) in a mixture of $\text{Zr}(\text{MesPDP}^{\text{Ph}})_2$ and DPA in deaerated THF. The red line is the kinetic fit to Eq. S3 and the blue line is the residuals of the fit.

Table S2 Kinetic parameters obtained from the fits to the sensitized DPA transient absorption decays at 450 nm to the Eq S3.

Pulse Energy (mJ)	$[{}^3\text{A}^*]$ (10^{-6}M)	α (10^3 s^{-1})	β	k_{T} (10^3 s^{-1})	k_{TTA} ($10^9\text{ M}^{-1}\text{ s}^{-1}$)
1.0	1.19	6.68	0.829	1.38	5.64
1.8	1.69	8.36	0.861	1.35	4.96
2.3	1.97	9.50	0.880	1.30	4.81
3.4	2.40	10.92	0.894	1.30	4.55
4.6	3.41	17.6	0.950	0.928	5.16

Table S3 Kinetic parameters obtained from the fits to the sensitized CzPA transient absorption decays at 430 nm to the Eq S3.

Pulse Energy (mJ)	$[{}^3\text{A}^*]$ (10^{-6}M)	α (10^3 s^{-1})	β	k_{T} (10^3 s^{-1})	k_{TTA} ($10^9\text{ M}^{-1}\text{ s}^{-1}$)
0.5	1.05	2.09	0.418	2.92	2.00
1.1	2.08	3.94	0.586	2.78	1.89
1.4	2.36	4.35	0.592	3.00	1.84
2.0	2.79	5.19	0.638	2.95	1.86
3.9	3.64	5.94	0.658	3.09	1.63

Table S4 Kinetic parameters obtained from the fits to the sensitized F-CzPA transient absorption decays at 430 nm to the Eq S3.

Pulse Energy (mJ)	[³ A*] (10 ⁻⁶ M)	α (10 ³ s ⁻¹)	β	k _T (10 ³ s ⁻¹)	k _{TTA} (10 ⁹ M ⁻¹ s ⁻¹)
0.6	0.90	2.24	0.464	2.59	2.50
1.5	2.33	3.97	0.596	2.69	1.71
3.3	3.29	4.87	0.605	3.18	1.48
3.9	3.49	5.48	0.659	2.84	1.57
4.4	3.64	4.86	0.611	3.09	1.34

Table S5 Kinetic parameters obtained from the fits to the sensitized CN-CzPA transient absorption decays at 430 nm to the Eq S3.

Pulse Energy (mJ)	[³ A*] (10 ⁻⁶ M)	α (10 ³ s ⁻¹)	β	k _T (10 ³ s ⁻¹)	k _{TTA} (10 ⁹ M ⁻¹ s ⁻¹)
0.6	1.05	4.00	0.769	1.20	3.79
0.9	1.68	4.56	0.758	1.46	2.72
2.1	3.13	6.60	0.780	1.86	2.11
3.1	3.62	6.90	0.754	2.25	1.91
3.6	3.82	6.86	0.729	2.55	1.80

Extrapolation of the Theoretical Power Density Threshold (I_{th}): The transition from quadratic to linear incident light power dependence has been characterized as the threshold intensity, I_{th}. Monguzzi and co-workers^{11,12} proposed a model equation of I_{th} expressed by Eq. S5 based on a simple kinetic rate modeling of the triplet acceptors' first-order decay rate and second-order TTA rate.

$$I_{th} = \frac{(k_T)^2}{\Phi_{TTET} \alpha k_{TTA}} \quad (S5)$$

where k_T denotes the first-order decay rate of acceptor triplets, Φ_{TTET} denotes the quantum efficiency of triplet energy transfer from the sensitizer to the acceptor, α denotes the absorption coefficient of the sensitizer at the excitation wavelength, and k_{TTA} denotes the second-order rate constant characterizing the TTA process. The k_{TTA} is related to the triplet diffusion coefficient and the effective triplet-triplet interaction distance in the fluid solutions.^{11,13} It should be noted that only the kinetics of the first- and second-order decay rate of acceptor triplets are considered in this model equation. Many other factors controlling the upconversion efficiency and I_{th} are not included in this expression, such as back energy transfer, concentration of sensitizer, TTA efficiency, etc.¹⁴⁻¹⁶ Therefore it is difficult to model different upconversion systems under various experimental conditions by directly using Eq. S5 without any corrections with other factors influencing I_{th}. However, for the same sensitizer/acceptor upconversion system, this model equation reveals a relationship between I_{th} and the relevant parameters in Eq. S5. The I_{th} is inversely proportional to Φ_{TTET} and α, where α is proportional to optical density (OD) at the excitation wavelength.

Extrapolation of the I_{th} value for the Zr(IV)/DPA system under optimized conditions (Φ_{TTET} = 95% and OD_{514 nm} = 0.2) is based on two experimental I_{th} values measured under two

distinct non-optimized quenching conditions shown in Fig. S10. For the same sensitizer/acceptor upconversion composition, k_T and k_{TTA} are both dependent only on the acceptor triplets, thus regarded constant for the same upconversion compositions.

$$\frac{I_{th,opt}}{I_{th,non-opt}} = \frac{\Phi_{TTET, non-opt}}{\Phi_{TTET, opt}} \times \frac{OD_{514nm, non-opt}}{OD_{514nm, opt}} \quad (S6)$$

For the Zr(IV)/DPA pair under non-optimized quenching conditions in Fig. S10 A, $\Phi_{TTET} = 14\%$, $OD_{514nm} = 0.05$, and the experimental I_{th} was 2.31 mW/cm^2 . The calculated $I_{th,opt} = 0.077 \text{ mW/cm}^2$ is given by

$$\frac{I_{th,opt}}{2.31 \text{ mW/cm}^2} = \frac{14\%}{95\%} \times \frac{0.05}{0.20}$$

When $\Phi_{TTET} = 50\%$, $OD_{514nm} = 0.08$, the experimental I_{th} was 0.72 mW/cm^2 as shown in Fig. S10 B. The calculated $I_{th,opt} = 0.152 \text{ mW/cm}^2$ is given by

$$\frac{I_{th,opt}}{0.72 \text{ mW/cm}^2} = \frac{50\%}{95\%} \times \frac{0.08}{0.20}$$

Therefore the approximate “calculated” I_{th} value for the Zr(IV)/DPA upconversion pair with $\Phi_{TTET} = 95\%$, $OD_{514nm} = 0.20$ is reported as an average of 0.077 and 0.152 mW/cm^2 , yielding a calculated $I_{th} = 0.115 \pm 0.038 \text{ mW/cm}^2$, which is below the detection limit of the power densities utilized ($\sim 0.38 \text{ mW/cm}^2$) and is qualitatively consistent with the experimental results.

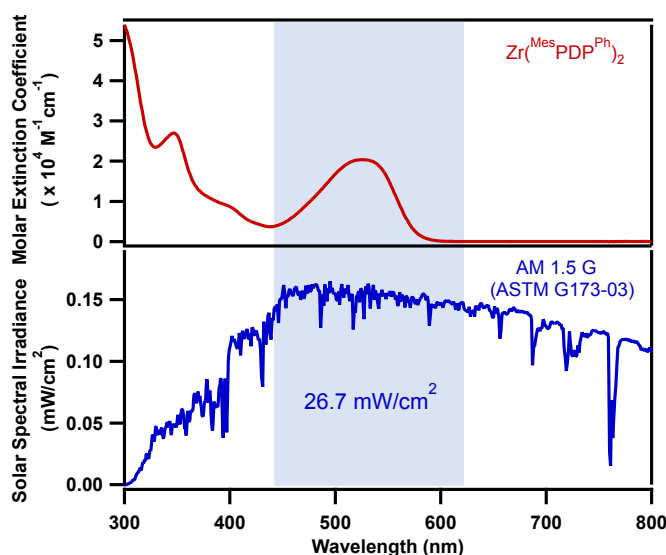


Fig. S21. Molar extinction coefficient of $Zr^{(MesPDPPh)}_2$ as a function of wavelength (top) and the AM 1.5 G (ASTM G173-03) solar spectral irradiance over UV and visible wavelengths (bottom).¹⁷ The blue shaded area (443 – 610 nm) indicates the lowest energy absorption band of $Zr^{(MesPDPPh)}_2$, over which the integrated solar irradiance is 26.7 mW/cm^2 , larger than the 13 mW/cm^2 value where maximum η_{UC} was realized for each UC composition.

References

1. Y. Zhang, T. S. Lee, J. M. Favale, D. C. Leary, J. L. Petersen, G. D. Scholes, F. N. Castellano and C. Milsmann, *Nature Chem.*, 2020, **12**, 345–352.
2. Y. Huang, X. Du, S. Tao, X. Yang, C.-J. Zheng, X. Zhang and C.-S. Lee, *Synth. Met.*, 2015, **203**, 49–53.
3. W. Liu, S. Ying, R. Guo, X. Qiao, P. Leng, Q. Zhang, Y. Wang, D. Ma and L. Wang, *J. Mater. Chem. C*, 2019, **7**, 1014–1021.
4. F. Deng, J. Blumhoff and F. N. Castellano, *J. Phys. Chem. A*, 2013, **117**, 4412–4419.
5. K. A. E. Roz and F. N. Castellano, *Chem. Commun.*, 2017, **53**, 11705–11708.
6. T. N. Singh-Rachford and F. N. Castellano, *Coord. Chem. Rev.*, 2010, **254**, 2560–2573.
7. S. M. Bachilo and R. B. Weisman, *J. Phys. Chem. A*, 2000, **104**, 7711–7714.
8. A. Haefele, J. Blumhoff, R. S. Khnayzer and F. N. Castellano, *J. Phys. Chem. Lett.*, 2012, **3**, 299–303.
9. Y. Y. Cheng, B. Fückel, T. Khoury, R. G. C. R. Clady, M. J. Y. Tayebjee, N. J. Ekins-Daukes, M. J. Crossley and T. W. Schmidt, *J. Phys. Chem. Lett.*, 2010, **1**, 1795–1799.
10. I. Carmichael, W. P. Helman and G. L. Hug, *J. Phys. Chem. Ref. Data*, 1987, **16**, 239–260.
11. A. Monguzzi, J. Mezyk, F. Scotognella, R. Tubino and F. Meinardi, *Phys. Rev. B Condens. Matter Mater. Phys.*, 2008, **78**, 195112.
12. A. Monguzzi, R. Tubino, S. Hoseinkhani, M. Campione and F. Meinardi, *Phys. Chem. Chem. Phys.*, 2012, **14**, 4322–4332.
13. J. Jortner, S. Choi, J. L. Katz and S. A. Rice, *Phys. Rev. Lett.*, 1963, **11**, 323–326.
14. E. M. Gholizadeh, L. Frazer, R. W. MacQueen, J. K. Gallaher and T. W. Schmidt, *Phys. Chem. Chem. Phys.*, 2018, **20**, 19500–19506.
15. N. A. Durandin, J. Isokuortti, A. Efimov, E. Vuorimaa-Laukkanen, N. V. Tkachenko and T. Laaksonen, *J. Phys. Chem. C*, 2019, **123**, 22865–22872.
16. D. Meroni, A. Monguzzi and F. Meinardi, *J. Chem. Phys.*, 2020, **153**, 114302.
17. General Information on the PVEducation. *Standard Solar Spectra*, www.pveducation.org/pvc/drom/appendices/standard-solar-spectra.